Journal of Power Sources 245 (2014) 796–800

Contents lists available at SciVerse ScienceDirect

Journal of Power Sources

journal homepage: www.elsevier.com/locate/jpowsour

Short communication

Implications of polymer electrolyte fuel cell exposure to synchrotron radiation on gas diffusion layer water distribution

Jens Eller [a], Jörg Roth [a], Federica Marone [b], Marco Stampanoni [b,c], Alexander Wokaun [a], Felix N. Büchi [a,*]

[a] Electrochemistry Laboratory, Paul Scherrer Institut, Villigen PSI, Switzerland
[b] Swiss Light Source, Paul Scherrer Institut, Villigen PSI, Switzerland
[c] Institute for Biomedical Engineering, University and ETH Zurich, Zurich, Switzerland

HIGHLIGHTS

- In-situ synchrotron based X-ray tomographic microscopy of water in PEFC.
- Studied influence of X-ray irradiation on water saturation.
- Absorption of 3.5 J cm^{-2} X-ray energy clearly distorts current and water distribution.
- Measurement bias difficult to detect as water distribution patterns remain similar.

ARTICLE INFO

Article history:
Received 12 April 2013
Received in revised form
19 June 2013
Accepted 5 July 2013
Available online 13 July 2013

Keywords:
Polymer electrolyte fuel cell (PEFC)
Gas diffusion layer
Water saturation
X-ray tomographic microscopy
Synchrotron imaging
Measurement bias

ABSTRACT

Synchrotron radiation (SR) based imaging of polymer electrolyte fuel cells (PEFC), both radiography and tomography, is an attractive tool for the visualization of water in the gas diffusion layer as it provides temporal and spatial resolutions one order of magnitude superior to neutron imaging. Here we report on the degradation of cell performance and changes in GDL water saturation after SR irradiation of about 43% of a cell's active area. Fast X-ray tomographic microscopy (XTM) scans of 11 s duration are used to compare the GDL saturation before and after a 5 min irradiation period of the imaged section. The cell voltage and the water saturation decreased clearly during and after the exposure. Estimates of the current density of the SR exposed and non exposed cell domains underline the effect of irradiation.

© 2013 Elsevier B.V. All rights reserved.

1. Introduction

X-ray tomographic microscopy (XTM) has proven to be a valuable tool to study the water transport paths in the gas diffusion layers (GDL) of polymer electrolyte fuel cells (PEFC) [1–7] in order to improve the water management and power density.

Though the effects of high energy radiation are well known in the field of radiation chemistry (see e.g. O'Donnell [8]) and Schulze et al. [9] have shown already in 1999 how Nafion degrades during XPS analysis, the consequences of X-ray exposure on PEFC operation remain unclear and are rarely discussed in the electrochemical literature on X-ray imaging [3,7,10–12]. This work intends to show, how X-ray induced PEFC performance degradation biases the water distribution measured via XTM. Additional to the XTM imaging, the cell performance after the imaging experiments is characterized and the sulfate release of ex-situ SR exposed catalyst coated membrane samples is analyzed by liquid ion chromatography to gain understanding of the sources of performance degradation.

2. Experimental

A single channel cell [3] designed for XTM investigations as shown in Fig. 1a was used. The active area of the catalyst coated membrane (CCM, 2-mil Nafion with Pt-loading 0.2/0.4 mg cm^{-2} from Umicore) was limited to 30 mm^2 by a polymer sub-gasket and the GDL (Toray TGP-H060 with MPL from Umicore, 2.3 mm width,

* Corresponding author.
E-mail address: felix.buechi@psi.ch (F.N. Büchi).

0378-7753/$ – see front matter © 2013 Elsevier B.V. All rights reserved.
http://dx.doi.org/10.1016/j.jpowsour.2013.07.025

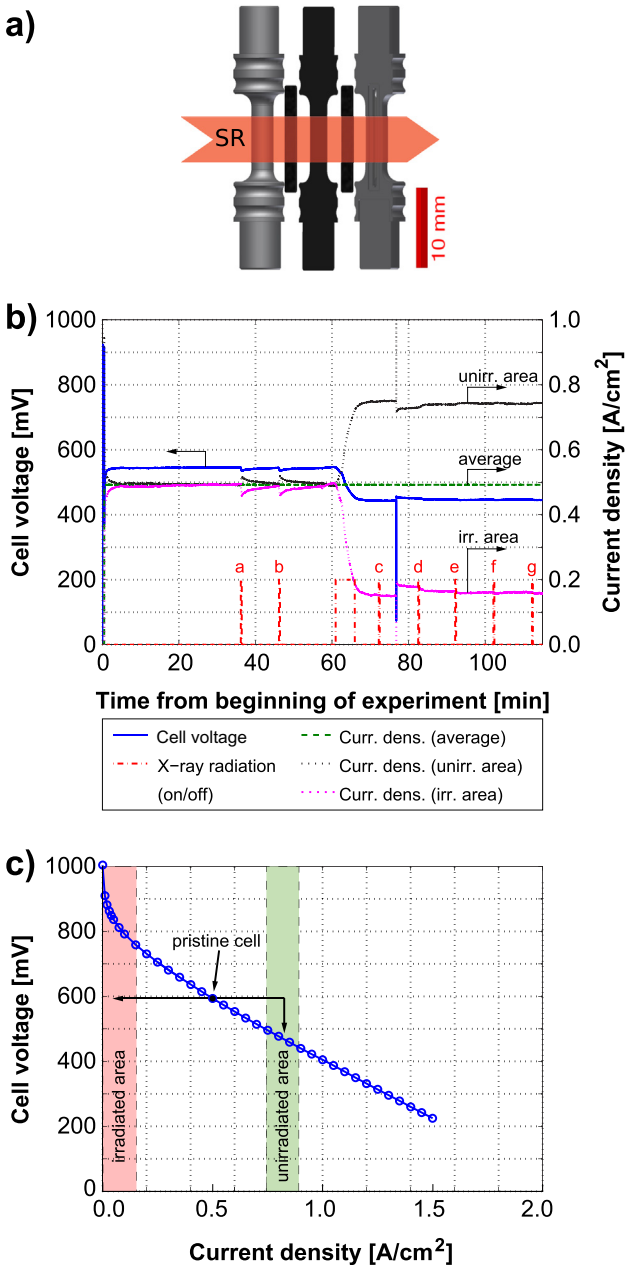

Fig. 1. a) Schematic of XTM-PEFC. Red arrow indicates the SR irradiated domain of the flow field, GDL and CCM (sub-gasket, heater and temperature sensors not shown); b) time series data of cell voltage, X-ray shutter state (zero means shutter closed), average cell current density, as well as current densities of SR irradiated and non-irradiated domains estimated from interpolated polarization curve data c) polarization curve of pristine cell (30 s current holding time); the deviation of 45 mV cell voltage at 0.5 A cm^{-2} before the SR exposure introduces an uncertainty of the current densities for the non-irradiated (light green area) and for the irradiated area (light red area) after the SR exposure. (For interpretation of the references to color in this figure legend, the reader is referred to the web version of this article.)

13.4 mm length). The cell was operated at a temperature of 35 °C with hydrogen/oxygen feed humidified at room temperature (40% relative humidity) with gas velocities of 0.56 m s^{-1} at the cathode and 1.1 m s^{-1} at the anode (stoichiometries > 10).

XTM imaging experiments were performed at the TOMCAT beamline of the Swiss Light Source (SLS) at Paul Scherrer Institut, Switzerland [13]. A pco.Dimax camera was used for fast tomographic scans (180° sample rotation, 1001 projections, 11 ms exposure time per projection, 11 s total scan time) at 13.5 keV monochromatic beam energy and a beam height of 5.6 mm. The beam photon flux[1] of 6×10^{13} ph (s cm^2)$^{-1}$ at 13.5 keV corresponds to an energy flux of 130 mW cm^{-2}. The maximum magnification of the zoom objective microscope resulted in 2.95 μm pixel edge length.

At the beamline, the cell was operated at a constant current of 150 mA (0.5 A cm^{-2} average) for 60 min before the irradiation experiment, with the cell voltage being stable during operation for the last 30 min. The imaged and SR irradiated center section of the cell consisted of 43% (12.9 mm^2) of the overall active area. During the SR irradiation period of 300 s (5 min) the membrane electrode assembly (MEA) was oriented perpendicular to the beam.

The CCM has an absorbance factor of 0.125 [11]. It accumulates in total an X-ray energy of 3.3 J cm^{-2} (10.9 mW cm^{-2}) during the 300 s irradiation and about 0.1 J cm^{-2} during a single fast XTM scan, taking into account the reduction of the beam intensity due to the cell components between the X-ray source and the CCM.

Before and after the extended SR irradiation period of 300 s, fast XTM scans were taken to study the water distribution in the SR irradiated area. To measure the unbiased water distribution, two XTM scans were performed 25 and 15 min before the SR irradiation, labeled as scan a and b, respectively. 6 min after the SR irradiation the cell was scanned (scan c) and then every 10 min following the water development of the water distribution for 46 min (scans d to g). The degradation of cells at 30 °C from few fast XTM scans, accumulating up to 60 s exposure time at TOMCAT (absorbed X-ray energy of 0.7 J cm^{-2} at the CCM), can be regarded as negligible [7].

Image segmentation was done as described in Ref. [3] but limited to liquid water as in Ref. [7] because the overall solid segmentation was prevented by inhomogeneities of the gray scale values in the MPL domain due to the strong absorption of the catalyst layer.

As the X-ray irradiation of the cell causes a performance degradation of the irradiated domain [10], the current of the irradiated domain (I_{irr}) will decrease. Since the cell is operated in constant current mode, the current of the unirradiated cell area (I_{unirr}) has to increase accordingly to maintain the overall cell current (I_{tot}), as it holds:

$$I_{tot} = I_{irr} + I_{unirr} \quad (1)$$

Under the assumption of a homogeneous cell voltage (E) over the whole MEA area, the current density of the non-SR exposed cell area and I_{unirr} can be estimated using an interpolation of the cells pristine polarization curve data ($i_{prist}(E)$)

$$I_{unirr} = i_{prist}(E) \times A_{unirr} \quad (2)$$

where A_{unirr} is the unirradiated cell area of 17.1 mm^2. Rearranging Eq. (1) and inserting Eq. (2) gives an estimate of I_{irr}, that can be converted into an estimation of the current density of the irradiated cell area (i_{irr}) knowing the irradiated cell area (A_{irr} = 12.9 mm^2)

$$i_{irr} = \frac{I_{tot} - i_{prist}(E) \times A_{unirr}}{A_{irr}} \quad (3)$$

[1] The values of the beam energy flux and of the absorbed X-ray energy reported here are higher than those reported by Roth et al. [11]. This is because in Ref. [11] a more conservative estimate of the beam intensity of 1×10^{13} ph (s cm^2)$^{-1}$ at 13.5 keV was used.

A Metrohm 882 Compact IC plus equipped with a Metrosep A Supp 5–150 column was used for ion chromatography measurements of the sulfate release of pristine and irradiated CCM samples. CCM samples with an area of 4 × 20 mm^2 where completely irradiated at 13.5 keV for 6 and 60 s with the setup as described by Roth et al. [11]. The pristine and irradiated samples were placed into de-ionized water at 80 °C for at least 6 h. Similar as reported in Ref. [11], small pieces of catalyst layer detached from the CCM, especially after 60 s of SR exposure. Therefore each sample water was filtered before the ion chromatography measurement to remove detached catalyst layer particles.

3. Cell performance degradation

Within this section the influence of the partial irradiation of the MEA to the synchrotron radiation on the cell voltage during constant current operation is discussed and estimates of the current densities of the irradiated and non-irradiated MEA areas are provided.

During the scans a and b the cell lost about 10 mV in cell voltage each, but recovered to the initial value within 10 min (see Fig. 1b). During the 300 s SR irradiation the cell voltage decreased from 547 mV to about 455 mV. Thereafter, the cell voltage stabilized at 444 mV showing an obvious performance degradation. Similar voltage loss of a partially SR irradiated cell has been reported by our group already in 2011 [3].

Based on the polarization curve of the pristine cell (see Fig. 1c) and Eq. (3), the non-irradiated MEA current density can be estimated to increase to about 0.75 A cm^{-2}. Correspondingly, the current density of the SR irradiated MEA can be estimated to decrease to a value around 0.15 A cm^{-2} (see Fig. 1b). During the scans after the SR irradiation, cell voltage and current density distribution did not change obviously, indicating that the performance degradation has reached a stable value with the SR irradiated area being not completely inactive.

It has to be mentioned, that an offset of 45 mV cell voltage exists at 0.5 A cm^{-2} between the polarization curve pre-characterization (592 mV) and the cell voltage at the beamline (547 mV). It is mainly caused by an additional clamping on the flow fields, which was applied during the polarization curve measurement but that could not be applied at the beamline. The cell voltage used in Eq. (2) is corrected for this offset such that the estimates of current densities of the irradiated and unirradiated domains match the overall current density of 0.5 A cm^{-2} before the first XTM scan. The offset in cell voltage and its correction introduce some additional uncertainty to the current density estimates that is expressed in Fig. 1c by the green and red areas for the unirradiated and irradiated domains, respectively. However, the qualitative trend of the decreasing irradiated and increasing unirradiated MEA current density remains unaffected by this uncertainty.

Around minute 77 of the experiment at the beamline (see Fig. 1b) an error of the electronic load occurred for the fracture of a second. The cell voltage dropped for a short time to below 100 mV and the precise current remains unclear. Thereafter, the cell voltage was about 15 mV higher than before minute 77, but slowly equilibrated again to 545 mV. The resulting deviation of the local current density estimates are likely artifacts of an unequilibrated cell voltage.

Different reasons for the X-ray induced performance losses are discussed in the literature, ranging from perturbed water management due to reduced water contact angles [10,11], loss of membrane sulfonation [10,11], catalyst poisoning by membrane decomposition products [10,11], mechanical damage of the catalyst layer [11], or dry out of ionomer related to cell heat up [12].

Table 1
Sulfate release and absorbed X-ray energy of ex-situ SR exposed CCM samples.

Exposure time [s]	Absorbed X-ray energy [J cm^{-2}]	Sulfate release [μmol g^{-1}]
0	0	25.4
6	0.1	35.5
60	1.0	53.6

The X-ray energy flux that is absorbed in the CCM (10.9 mW cm^{-2}) is comparatively low in relation to the electrochemical losses of about 300 mW cm^{-2} at the chosen operation point. It is therefore unlikely that cell heat-up due to beam absorption causes a significant dry-out of membrane and catalyst layer ionomer that would explain the observed loss in cell voltage as suggested by Ref. [12].

The catalyst poisoning hypothesis is supported by an increased sulfate release that was observed for ex-situ exposed CCM samples (see Table 1). The sulfate release of the CCM samples is more than doubled already after 60 s of SR irradiation. Sulfate is a strong platinum catalyst poison, that can be removed from the catalyst at least partially during cell operation [14,15]. A partial recovery of cell performance was observed during post-irradiation characterization of the irradiated cell with the additional flow field clamping mounted again. After post-characterization operation for 16 h, the cell voltage was only 19 mV lower at 0.5 A cm^{-2} during polarization curve measurement (30 s current holding time) than for the pristine cell compared to about 100 mV directly after the irradiation.

Furthermore, the cell voltage deviates clearly for the irradiated cell during post-characterization for different current holding times (30 s or 30 min), whereas there was no or only minor deviation (<5 mV) over a wide range of current densities for the pristine cell (see Table 2). This effect seems to be related to the reduced contact angles of the GDL and the catalyst layer, which might lead to an accumulation of liquid water in the electrodes and an increased mass transport overpotential.

From the authors point of view a combination of (i) catalyst poisoning (especially by sulfur species), (ii) perturbed water management due to reduced contact angles of GDL and catalyst layer [11], and (iii) mechanical destabilization of the catalyst layer [11] remain as the most probable sources of the reduced current density in the imaged section, but the share of their contributions remains unclear.

4. XTM results

This section shows how the biased current density distribution affects the depicted water distribution qualitatively and quantitatively. Only the cathode GDL is analyzed as the anode GDL was found dry.

The visual inspection of the raw XTM in-plane (IP) slices, that are parallel to the membrane, shows clearly a reduced water saturation in the GDL after the SR irradiation (see Fig. 2). Most of

Table 2
Cell voltage at 0.25 and 1.0 A cm^{-2} before and after SR exposure for different current holding times, as well as the absolute deviation of the cell voltage |ΔU|.

Current holding time	0.25 A cm^{-2}		1.0 A cm^{-2}	
	Pristine	Irradiated	Pristine	Irradiated
30 s	705 mV	693 mV	405 mV	378 mV
30 min	709 mV	679 mV	404 mV	348 mV
|ΔU|	4 mV	14 mV	1 mV	35 mV

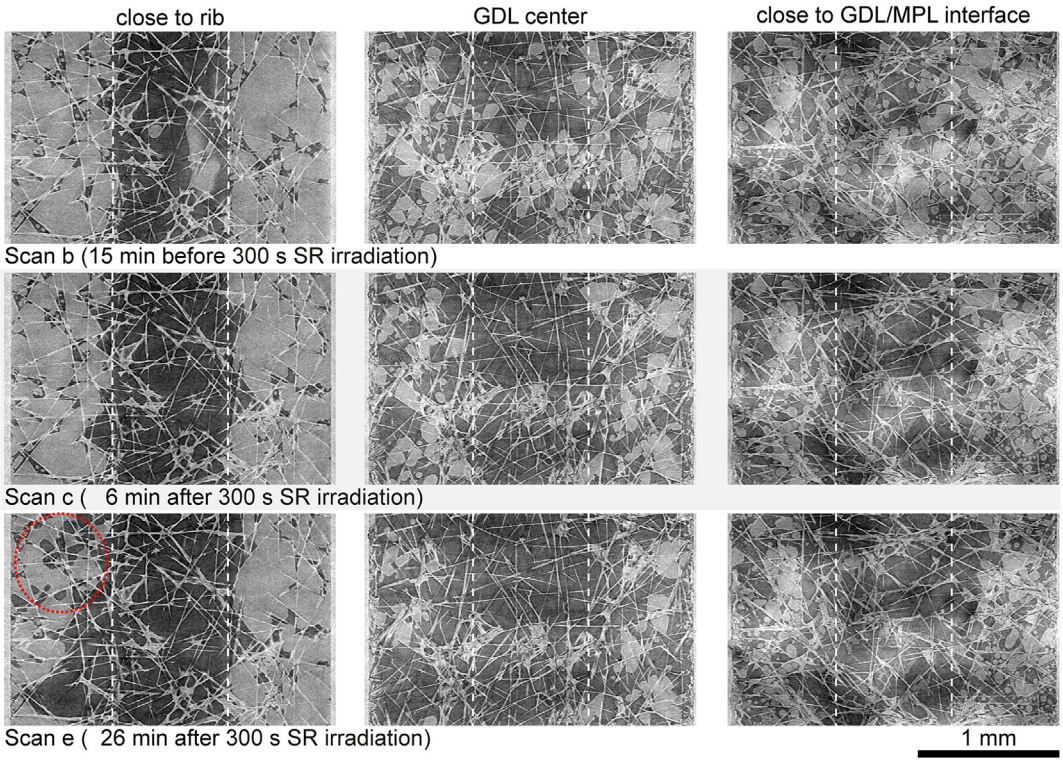

Fig. 2. In-plane ortho-slices (parallel to the membrane) of scan b, c, and e close to the GDL-rib interface (left column), in the center of the GDL (mid column), and close to the MPL (right column) at position 3.1–4.6 mm of Fig. 3; white dashed lines indicate the position of the flow field rib edges; gray scales of IP-slices close to MPL are disturbed due to blurring from catalyst layer inhomogeneities; red dotted ellipse indicates GDL domain, where concave menisci of receding water front can be observed. (For interpretation of the references to color in this figure legend, the reader is referred to the web version of this article.)

the water distribution patterns in the teflonated GDL remain similar after SR irradiation, though at lower saturation levels. Concave water menisci that would clearly identify a receding water front can be localized only at rare locations close to the flow field ribs (i.e. in Fig. 2, scan e, left rib).

The temporal development of the liquid water volume fraction is quantified in Table 3 and Fig. 3. Before the 300 s SR irradiation the liquid water volume fraction stabilized at about 7% in the GDL channel domain and 35% in the GDL rib domain. 6 min after the SR irradiation the channel GDL was almost completely dry as the liquid water volume fraction had decreased to 1.5%. 40 min later the liquid water volume fraction of the channel GDL had reduced only slightly to 1.1%. The liquid water volume fraction under the ribs also decreases after SR irradiation, but after 46 min it is still 27% and the decrease flattens out.

In Fig. 3 it can be seen, how the cathode gas channel empties and that areas of high mean liquid water volume fraction are retained only under the center of the flow fields ribs. There, the liquid water content remains highest close to the flow field ribs. Only at the boundaries of the imaged section water paths into the channel domain of the GDL can be detected after the SR irradiation.

Table 3
Development of the liquid water volume fraction in the SR exposed area before (scans a and b) and after an extended irradiation period of 300 s with MEA ⊥ SR (scans c to g).

XTM scan	GDL liquid water volume fraction [%]	
	Channel	Ribs
a (25 min before 300 s irrad.)	7.3	34.7
b (15 min before 300 s irrad.)	7.1	35.2
c (6 min after 300 s irrad.)	1.5	32.1
d (16 min after 300 s irrad.)	1.3	29.2
e (26 min after 300 s irrad.)	1.2	27.8
f (36 min after 300 s irrad.)	1.0	27.3
g (46 min after 300 s irrad.)	1.1	27.0

Because there is almost no contrast between liquid water and solid MPL, it remains unclear, if the water that is detected at the GDL/MPL-catalyst layer interface (not hot-pressed) accumulated in gaps between MPL and the catalyst layer or if it is an artifact of the dry–wet referencing during the image segmentation.

At a cell temperature of 35 °C the diffusive flux of water vapor through the GDL is strongly limited by the low partial pressure of water. At these conditions liquid water can be found in the GDL also under the channel even in the case of not fully saturated gases in the gas flow channels (scans a and b). As the current density of the imaged section is affected by the X-ray irradiation, the local water production becomes lower than the evaporation rate and the water saturation decreases (scans c and e) towards a new equilibrium (probably scans f and g).

Since the imaged area is only 5.6 mm high, flow of liquid water through the GDL from the non-degraded PEFC area into the degraded PEFC area could prevent stronger decrease of water saturation in the SR exposed area. This phenomenon is commonly discussed in porous media research and described as “stage 1” during drying of a porous media, where water is transported through paths within the connected liquid phase to the evaporation front (see e.g. Lehmann et al. [16]). The differences in the decrease of the water saturation under the ribs and along the channel seem to be related to different connectivity of the imaged water clusters to the non disturbed MEA domains. It is very likely that the water in the emptying regions was not connected to

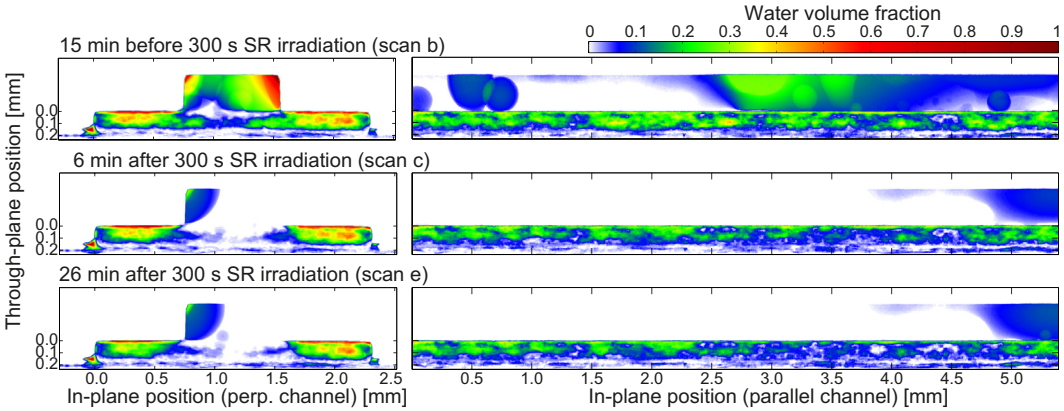

Fig. 3. Through-plane (perpendicular to the membrane) liquid water volume fraction projected parallel (left) and perpendicular (right) to the channel.

non-degraded MEA domains, while in the other domains the evaporation front stays stable due to water feed from non-degraded MEA domains.

5. Conclusion

During the partial exposure of an operating PEFC with synchrotron radiation for 300 s, that accumulates an absorbed X-ray energy of 3.3 J cm^{-2} at the CCM, a clear loss of cell performance was observed. The current density of the irradiated domain decreased, while the current density of the remaining cell increases in constant current operation. A combination of different processes (catalyst poisoning, perturbed water management and mechanical destabilization of the catalyst layer) seems to be source of the performance degradation in the imaged section and further investigations are currently ongoing to clarify this question.

The GDL water saturation was also biased by the irradiation and decreased both under ribs and channel of the imaged section. The structural patterns of the water clusters remained similar throughout most of the teflonated GDL besides some rare locations at the GDL-rib interface. Therefore, the biased current density and water distribution of the imaged section can not be identified from the XTM data, if the unbiased state is unknown.

If the active area of the cell is larger than the imaged section and the absorbed energy exceeds 3.5 J cm^{-2} at the given beam intensity and operating conditions, the water distribution measured by XTM will be affected by the method itself as the X-ray irradiation influences the local equilibrium of water production and removal. As the local current density is decreased, the channels relative humidity, which itself is set by the average upstream current density and the inlet humidities, becomes the major player. In case of not fully humidified gases in the channels a decreasing saturation due to evaporation will be observed, as reported here. If the gases in the channels of the imaged section are fully humidified, the liquid water saturation in the GDL might not change during and after the irradiation because evaporation is suppressed, or the liquid water saturation in the GDL becomes dominated by condensation of humidity from the channel. Then the local water saturation will correlate only indirectly to the cell's average current density by the channel's humidity and liquid water transport, but not by a response of the local current density.

An absorbed X-ray energy of 3.5 J cm^{-2} in the CCM can be regarded as reference where severe radiation induced changes of the electrochemical performance and liquid water distribution of the imaged section must be expected. The precise dose limit which should not be exceeded needs to be identified for each X-ray PEFC imaging setup, since cell design, orientation and operating conditions, as well as X-ray source characteristics can influence the radiation driven degradation processes.

Acknowledgment

Financial support from the Swiss Federal Office of Energy under grant no. 153708, precise machining work by M. Hottiger, software and electronic support by T. Gloor, and support during measuring campaign at the TOMCAT beamline by S. Kreitmeier and M. Citerne are gratefully acknowledged.

References

[1] P. Sinha, P. Halleck, C.-Y. Wang, Electrochem. Solid-State Lett. 9 (2006) A344–A348.
[2] F.N. Büchi, R. Flückiger, D. Tehlar, F. Marone, M. Stampanoni, ECS Trans. 16 (2008) 587–592.
[3] J. Eller, T. Rosén, F. Marone, M. Stampanoni, A. Wokaun, F.N. Büchi, J. Electrochem. Soc. 158 (2011) B963–B970.
[4] P. Krüger, H. Markötter, J. Haussmann, M. Klages, T. Arlt, J. Banhart, C. Hartnig, I. Manke, J. Scholta, J. Power Sources 196 (2011) 5250–5255.
[5] H. Markötter, I. Manke, P. Krüger, T. Arlt, J. Haussmann, M. Klages, H. Riesemeier, C. Hartnig, J. Scholta, J. Banhart, Electrochem. Commun. 13 (2011) 1001–1004.
[6] R. Flückiger, F. Marone, M. Stampanoni, A. Wokaun, F.N. Büchi, Electrochim. Acta 56 (2011) 2254–2262.
[7] J. Eller, J. Roth, F. Marone, M. Stampanoni, A. Wokaun, F.N. Büchi, ECS Trans. 41 (2011) 387–394.
[8] J.H. O'Donnell, ACS Symposium Series, vol. 381, American Chemical Society, Washington, DC, pp. 1–13.
[9] M. Schulze, M. Lorenz, N. Wagner, E. Gülzow, J. Fresenius, Anal. Chem. 365 (1999) 106–113.
[10] A. Schneider, C. Wieser, J. Roth, L. Helfen, J. Power Sources 195 (2010) 6349–6355.
[11] J. Roth, J. Eller, F.N. Büchi, J. Electrochem. Soc. 159 (2012) F449–F455.
[12] C. Hartnig, I. Manke, Woodhead Publishing Series in Energy, vol. 2, Woodhead Publ., Cambridge, UK, pp. 462–482.
[13] F. Marone, R. Mokso, P. Modregger, J. Fife, B. Pinzer, T. Thuring, K. Mader, G. Mikuljan, A. Isenegger, M. Stampanoni, AIP Conf. Proc. 1365 (2011) 116–119.
[14] A. Kabasawa, H. Uchida, M. Watanabe, Electrochem. Solid-State Lett. 11 (2008) B190–B192.
[15] A. Kabasawa, J. Saito, K. Miyatake, H. Uchida, M. Watanabe, Electrochim. Acta 54 (2009) 2754–2760.
[16] P. Lehmann, S. Assouline, D. Or, Phys. Rev. E 77 (2008) 056309.